Radiation Detection Technology and Methods (2023) 7:465–483
https://doi.org/10.1007/s41605-023-00426-9

REVIEW

A review on emerging materials with focus on BiI_3 for room-temperature semiconductor radiation detectors

Ritu Chaudhari[1] · Chhaya Ravi Kant[1] · Alka Garg[2] · Surender Kumar Sharma[3]

Received: 22 March 2023 / Revised: 15 September 2023 / Accepted: 5 October 2023 / Published online: 24 November 2023

Abstract

Purpose Considerable advances in the fundamental knowledge and applications of radiation science have led to significant progress and development of room-temperature semiconductor radiation detectors (RTSD). The RTSDs technologies are continuously evolving with accelerated research and material engineering in the last decade. Significant scientific and technological advancements have led to development of high-performance radiation detectors with high signal-to-noise ratio (SNR), better sensitivity, faster response and higher-resolution with capability of desired room-temperature operation. This paper is a review on emerging semiconductor radiation detector materials with a deeper insight into the prospective role of Bismuth tri-iodide (BiI_3) for room-temperature radiation detectors.

Methods An introduction of the state of art of most developed semiconductor materials, i.e., cadmium telluride (CdTe), mercury iodide (HgI_2), lead iodide (PbI_2), etc., and a critical examination of properties, shortcomings and challenges related to their synthesis have been elaborated. Polymer-semiconductor composites with desirable properties and their integration into detector devices is also presented. Subsequent sections discuss the role of BiI_3 as an emerging radiation detector material for room-temperature operation with an in-depth discussion on the role of defects in charge transportation and electrode configuration. Furthermore, the current challenges along with the future prospects of these materials for radiation detection to promote continuous innovation and practical applications are also elaborated.

Conclusion The comprehensive review on latest developments in room-temperature radiation detector materials is expected to help establish a technological roadmap for the synthesis, fabrication and commercialization of novel materials for development of efficient radiation detectors.

Keywords Radiation detector · Defects · Electrical properties · Bismuth tri-iodide · Semiconductor · Toxicity

Introduction

High-energy radiations promulgate immense modern day applications in varied fields like medical treatments, food preservation, security and defence, research laboratories, space stations, industries and many others [1]. Work environments dealing with high-energy radiations pose high risk of exposure due to leakage of radiations leading to deadly life-threatening diseases like cancer [2–4]. However, due to the danger of the leakage of radiations on human as well as environment, in future sometime soon world is going to face a new problem of radiation pollution at a large scale. It has not been possible to devise unerring, dependable and efficient ways to stop or contain the flow of leaked radiations and to monitor radioactive waste from research laboratories and factories which have resulted in dreadful accidents like Chernobyl disaster [5] and Delhi Mayapuri incident [6]. It is imperative to continuously monitor the level of these radiations in environment with real-time room-temperature dosimeters and sensors to control radiation pollution [7]. We already have a number of radiation detectors or sensors typically classified by the type of detector material, the source of radiation and the energy range of radiation. There are fundamentally three types of detectors in use for radiation detection applications: (1)

✉ Chhaya Ravi Kant
chhayaravikant@igdtuw.ac.in

[1] Department of Applied Sciences and Humanities, Indira Gandhi Delhi Technical University for Women, Kashmere Gate, Delhi 110006, India

[2] Gargi College, University of Delhi, Siri Fort Road, New Delhi 110049, India

[3] Delhi Skill and Entrepreneurship University, New Delhi, India

gas-filled detectors like GM counter, (2) scintillation detectors and (3) semiconductor detectors (solid-state detectors) [8, 11].

Gas-filled detectors are versatile and commercially used detectors in the market as they are cheap and have a long-life time. The gas-filled detectors operate on the basis of ionization of gas molecules by interaction of radiation. The operating voltage for gas detectors is in the range of 50–1000 V and in some cases even more than 1000 V depending on geometry of detector and energy of incident radiation [9, 10]. Despite being the major player in the market, gas detectors have certain limitations like low resolution, low sensitivity, high operation voltages and high recovery time [8, 9].

Second class of detectors, the scintillation detectors, are the oldest types of radiation detectors in which interaction of radiations with certain class of inorganic and organic scintillator materials leads to production of photons [11, 12]. This type of detector has high resolution and sensitivity compared to gas-filled detectors but the cost is much higher as scintillator materials are expensive and also the use of photomultiplier tube to enhance signals leads to an additional increase in the size and cost of detector [13]. However, due to electron–electron interactions in the material and potential barrier at the surface/vacuum interface, a considerable amount of energy loss of the order of 100 eV for generation of a single photoelectron occurs, which is much higher than the energy loss in gas-filled or semiconductor detectors [14] which reduces signal intensity or strength. Formation of F-centres and clusters in alkali and metal halides strongly affect the optical and structural properties of scintillators which affect the performance the device [15–17].

Third type of detectors are **solid-state detectors**, considered as contemporary and the future technology of detectors by experts [18]. Solid-state detectors have good resolution, sensitivity, room-temperature operation, compact size and good results observed at comparatively low voltages because of high density and absorption coefficient of semiconductor [19]. The resolution and response time for semiconductor detectors are also testified better than gas and scintillation detectors. These detectors generally have higher density than gas-filled detectors; thus, the diffusion affect is smaller, which results in an attainable resolution of less than 10 µm, and also, semiconductor detectors have low ionization energy (less than 10 eV for each e–hole pair) as compared to gas detectors (20–40 eV) and scintillators (400–1000 eV to create a photoelectron) [20]. The requisites for the functioning of a portable device detector are low bias voltage, high signal-to-noise ratio, room-temperature operation and lightweight, and these requisites can be congregated with various semiconductor detector materials. However, high cost, variation in material structure and properties, environmental degradation and performance deterioration pose certain limitations laying constraints on the use of semiconductor materials [22–27].

In this review, we have discussed about the properties, performance and limitations of the existing semiconductor materials for RTSD applications. Ideally a material with a high atomic number, high density and photoelectronic coefficient is required to develop a good RTSD (Fig. 1). To make the detector environment friendly, it is pertinent to choose a non-toxic and non-radioactive material for the detector fabrication. Thus, in the later sections of the review, authors have focussed on the potential of non-toxic BiI_3, possessing the desired properties to be a RTSD.

A comprehensive review of semiconductor detectors

Table 1 depicts series of common semiconductor materials which are explored as radiation detectors for detecting high radiations such as X-rays, gamma rays and alpha rays depending on their material characteristics like band gap, density, electron–hole pair creation or pair production energy, mobility-lifetime product (different for electrons and holes) and resistivity [18, 21–25].

The correlation matrix heatmap for the data in Table 1 is depicted in Fig. 2. The correlation matrix shows a significant dependence of resistivity on corresponding band gap which is quite expected as numbers of charge carriers depend on band gap. Further, a significant correlation exists between the resistivity and the corresponding density of material, the density of material which is an interesting correlation. A moderate negative correlation coefficient relates the electron mobility lifetime and the electron–hole pair production energy.

Semiconductor detectors are predominant and developing class of room-temperature radiation. These detectors can be further categorized into **three categories**, i.e. pure semiconductor detectors like silicon (Si), germanium

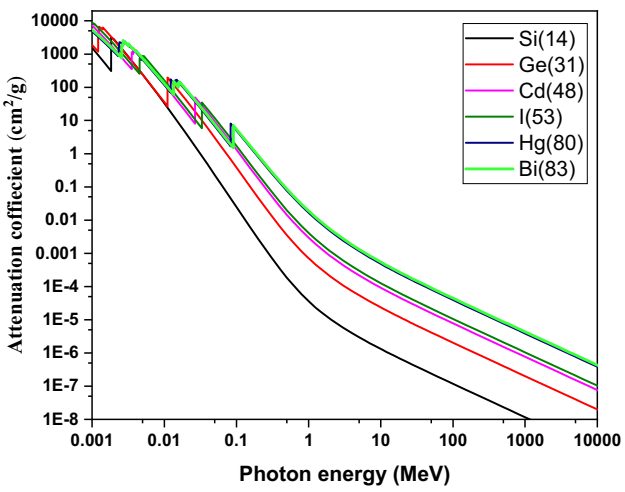

Fig. 1 Photoelectric attenuation of different semiconductors (showing variation with Z) at energy range of 0.1 keV to 10 GeV

Table 1 Properties comparison of potential semiconductor detector materials

Material	Atomic number (Z)	Band gap (eV)	Density	e–h pair production energy (eV)	$\mu\tau$ e^-	$\mu\tau$ h	Resistivity Ohm-cm	Toxicity level
Si	14	1.12	2.33	3.76	0.42	0.22	2.3×10^5	Low (2)
Ge	32	0.74	5.32	2.98	0.72	0.84	50	No
C (diamond)	6	5.4	3.5	13.25	2×10^{-5}	1.5×10^{-5}	$>10^{11}$	no
4H-SiC	14.6	3.24	3.20	7.78			2×10^{12}	low
SiC	14.6	2.2	3.12		10^{-6}	10^{-7}		Low (1)
CdTe	48.32	1.47	6.06	4.43	5×10^{-6}	5×10^{-6}	10^9	High (4)
CdZnTe	48.3052		6.02	4.5	5×10^{-4}	5×10^{-6}	10^{10}	high
CdZnSe	48.3054	2.0	5.50	6	10^{-4}		10^{10}	High (4)
CdSe	48.34	1.73	5.81	5.5	6.3×10^{-5}		10^{12}	High (4)
CdMnTe	48.2552	1.61	5.8	2.12	7×10^{-3}		10^{10}	High (4)
GaAs	31.33	1.36	5.36	4.51	1.2×10^{-5}	6×10^{-7}	10^7	High (danger)
Bi_2S_3	83.16	1.3	6.73		1.3×10^{-6}	7×10^{-7}		Very low (0)
HgI_2	80.53	2.13	6.36	4.2	10^{-4}	10^{-5}	10^{13}	High (3)
BiI_3	83.53	1.7	5.78	5.80	6×10^{-7}	10^{-7}	10^8–10^{11}	low (1)
PbI_2	82.53	2.6	6.16	7.68	2×10^{-7}	10^{-8}	10^{13}	High (4)
AlSb	13.51	1.62	4.26	5.055	10^{-6}	10^{-6}	10^8	High (4)
TlBr	81.35	2.68	7.5	7.7	3×10^{-4}	6×10^{-5}	10^{10}	Acute toxic
PbO	82.8	2.80	9.80	8.19	10^{-8}		10^{13}	
ZnO	30.8	3.38	5.61	8.37	10^{-4}–10^{-6}		3×10^{13}	

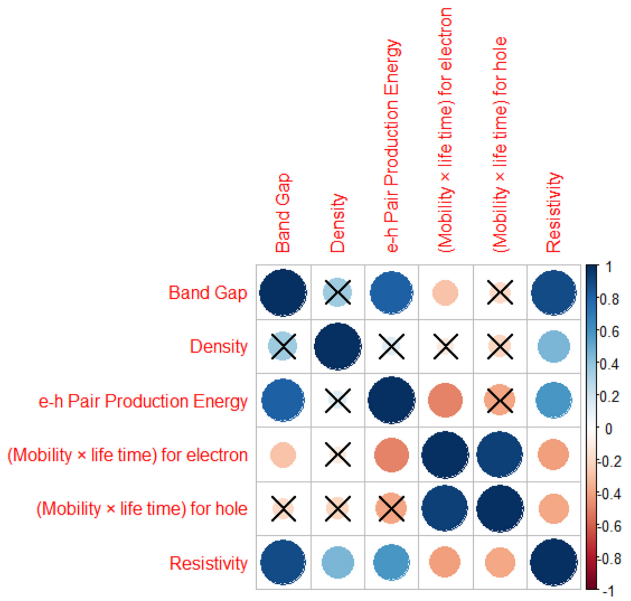

Fig. 2 Correlation matrix heatmap for physical parameters mentioned in Table 1

(Ge) [26]; compound semiconductor detectors based on cadmium (Cd)-based compounds [27], metal halides, etc. [28], and polymer–semiconductor composite-based detectors like cadmium telluride (CdTe)-polymer nanocomposites [27], polymer/CNT(carbon nanotubes)/high-Z composites, etc. [29, 30].

Pure semiconductor detectors

High density of silicon (2.329 g/cm^2) allows a moderate energy loss per unit length with detector thickness up to 300 µm apportioning a measurable signal-to-noise ratio as compared to other detectors with comparable thickness [31]. Also, silicon has a large industry presence with micro-chip technology, which makes it easy to design a detector [32]. Revelation of good resolution for tracking charged particles by silicon-based radiation detectors has made them mark their presence at the LHC in CERN detection system. Nevertheless, the major disadvantage of silicon detectors is their expensive cost as compared to cloud chambers or wire chambers, low atomic number and also degradation of the signal over time as a consequence of polarization due to radiations [33–35].

Another, semiconductor detector material most commonly used in detection is germanium due to its high atomic number and better photon interaction probability than Si. Germanium-based detectors do have good energy resolution and however require sophisticated cooling devices to operate at very low temperature of liquid nitrogen (− 196 °C), to reduce leakage currents and attain maximum efficiency which is major drawbacks of Ge detectors [33, 36, 44]. Eberth et al. devised a vacuum tight Ge detector

encapsulated in a thin (0.7 mm) aluminium encapsulated to avoid absorption of low-energy photons produced by Compton scattering leading to enhanced reliability and resolution (2.10 keV at 1.33 MeV) [36]. Despite these paybacks, the drawback of bulky cryogenic operation for a measurable signal-to-noise ratio was still persistent.

Diamond was identified as one such potential material for room-temperature radiation detection because of its high band gap (6 eV), high density and low leakage current [37, 46, 47]. An extremely low value 7.46×10^{-13} A/mm^2 for dark current was reported at an electric field of 1 V/μm by Kai Su et al. [38]. Due to high band gap of diamond, the detector thickness reduces and better signals can be observed when irradiated with ionizing radiations such as heavy ions, protons, alpha particles and intense gamma ray and X-ray beams at higher temperature [39]. Major disadvantages of diamond detectors are polarization of charge carriers and the exorbitant cost of diamond, even synthetic or artificial diamond are so expensive. Polarization in detector creates space charge accumulation which leads to creation of a dead zone in the detector leading to performance degradation [40].

Compound semiconductor detectors

Compound semiconductor materials need to possess a wide band gap, high density, etc., as minimum requirements to absorb the radiations and to produce a good response spectrum and be a good RTSD material. Some of most developed or explored compound semiconductor materials have been explored as promising materials for room-temperature radiation detectors and are summarized in Table 1. Silicon carbide (SiC) is a compound semiconductor which provides a number of advantages over silicon, i.e. ten times of the breakdown electric field strength, three times of the band gap, and permitting a wider range of *p*- and *n*-type control essential for device construction. But fabrication of SiC epitaxial layers thicker than 100 μm is cumbersome and expensive. Moreover, the operating voltage of the detector is higher than other available detectors [41]. 4H–SiC demonstrates promising results reported with best resolution spectra of 0.55% at 5.48 keV with thickness 15 micro-meter and bias voltage 40 V at room temperature and is stable in harsh environmental conditions befitting as the most ideal material for power devices [41].

Among all the compound semiconductor detectors, the most developed radiation detectors are undoubtedly cadmium-based compound detectors [42]. Cadmium telluride (CdTe) is considered as potential candidate for hard X-ray and gamma ray detection. The high atomic number (Z) of the material gives a high quantum efficiency in comparison with Si. However, a significant magnitude of charge loss arises due to low mobility and short lifetime of holes in these detectors which lowers the energy resolution [43]. Moreover, polarization affect lowers the performance of CdTe. Another compound CdSe has a broader forbidden band gap compared to CdTe, thus expounding lower intrinsic carrier concentration and leakage current [44, 45]. A ternary compound, cadmium zinc telluride (CZT), is synthesized by doping zinc (Zn) into the crystal of CdTe (generally 10% of Zn) to tailor the bandgap of the material. The doping with Zn improves resistivity of CZT by magnitude of the order of 2–3 as compared to CdTe and furthermore circumvents polarization affects after long periods of operation under bias voltage [46]. However, CZT suffers from high segregation coefficient of Zn and a significant compositional variation observed along the length leading to three major detrimental factors: compositional inhomogeneity forming new defect states, high concentration of dislocation walls/sub-grain boundary networks and high concentration of Te precipitates/inclusions which deteriorate the performance of CZT [22, 40]. These detrimental factors are mitigated by addition of selenium by the travelling heater method (THM) which promotes the growth of a new quaternary crystal having composition $Cd_{1-x}Zn_xTe_{1-y}Se_y$ (CZTS) as reported by Roy et al. [47]. The addition of Se has been reported to be very affective in minimizing the possibilities of formation of sub-grain boundaries and its networks, thus significantly minimizing the Zn segregation and ultimately improving the compositional homogeneity along the length of the grown ingots and resulting in much lower concentrations of Te inclusions/precipitates. Large CZT film array-based X-ray detector was synthesized by Xiuying Gao et al. as it is difficult to grow large crystals of CZT. This 8×8 array of X-ray detector shows high resistivity (3.33×10^{11} Ω cm) and fast photocurrent response for 35KVp X-rays [48].

Thallium bromide (TlBr) is another class of crystals extensively used for room-temperature X- and gamma rays detectors in 5 keV to 1 MeV energy range. This finds applications in space, medicine and also for radionuclide analysis [49]. The TlBr crystals have highest density (7.56 g/cm^3) among RTSD materials, high atomic number (81,35), wide band gap (2.68 eV), high mobility-lifetime product (10^{-3} cm^2/Vs) and higher resistivity at the expense of a marginally higher e–h pair creation energy [47]. TlBr marks certain band gap trap states from point defects that are predominantly neutral and badge the Fermi energy level near the middle of the band gap which helps retain high resistivity in the crystal [23]. But despite excellent advantages, this material is soft which makes it difficult to cut high quality crystals and also faces polarization issue over long period of usage under bias [50, 51].

Another potential RTSD material is mercury iodide (HgI_2) which was used for gamma ray spectrometer applications for the first time in 1971 [52]. The fabricated HgI_2 dosimeters have sufficient reproducibility and dose linearity for gamma rays that can be used as real-time monitoring system [53].

The detection range for HgI_2 crystals varies over a large span from low-energy X-rays of about 1.5 keV to high-energy gamma ray detection of up to 1332 keV [54]. But, material also has shortcomings, viz. low hole mobility, short mean free path for carriers, polarization, high leakage current and surface degradation of material with time [55]. Toxicity of mercury is also a major concern of HgI_2 semiconductor material [56]. Lead Iodide (PbI_2) is also considered as a potential RTSD candidate having amazingly high photoelectric efficiency and high atomic number [57, 58]. It has numerous advantages over HgI_2 detector. Material has high stability and does not undergo any phase transformation at high temperatures unlike HgI_2 growth restrained due to its inherent phase transition from orthorhombic to tetragonal phase at a temperature of 130 °C [59]. Lund et al. [60] have reported that PbI_2 detectors show a good energy resolution of 915 eV FWHM at 5.9 keV at room temperature. Also, through literature survey [61] it was found that PbI_2 detectors reveal an energy resolution of < 1 keV FWHM for 5.9 keV gamma rays. But major problem with PbI_2 detectors is its lead toxicity which makes its practical applications precarious for human beings [62]. Besides being toxic, the material is soft, difficult to grow, has polarization affects and exists in many phases which makes it difficult to handle [58, 63]. Some metal oxides like zinc oxide (ZnO) and lead oxide (PbO) fall under the category of highly resistive semiconductors and show promising results for detection of hard radiations. The ZnO single crystal has reported resistivity up to 10^{13} Ω cm (mentioned in Table 1) due to the reparation of the donor defects (V_O) and acceptor defects (V_{Zn} and O_i) after high-temperature annealing in oxygen for 1 hour. The O vacancy in material decreased with heating at a temperature of 250 °C in low vacuum [64]. The response time and recovery time for X-ray is reported in ns, which makes the material a good option for ultrafast detectors [65]. But, affective atomic number of ZnO is low, which makes the detector less suitable for high-energy X-rays or gamma rays. PbO also has good properties for semiconductor radiation detector but gives better results as direct inversion imaging scintillators [66]. However, the grain and defect density of ZnO can be controlled by varying thickness [67, 68].

Polymer-semiconductor composite detectors

The most common drawbacks of radiation systems for the detection as well as dosimetry of high-energy ionizing radiations are considered as low real-time signal, cost intensive and complicated synthesis process, need of cryogenic cooling for suppressing the dark current, less sensitivity to low-energy ionizing radiations, large and bulky size [69] which can be resolved to a certain extent by polymer-semiconductor composite-based detector materials. Since long, polymers have shown their presence in radiation applications like shielding, due to their expedient properties like better mechanical strength, high resistivity, low weight, low cost, environmental stability and flexibility [70]. However, polymers in isolation do not have good attenuation coefficient or high photon stopping power. Composites of polymers blend with clay, MWCNT, metals and high-Z semiconductors have been reported as a new emerging class of materials with advanced properties of polymers as well as semiconductors suitable for radiation detectors [71–74]. These fillers in polymer matrix downscale the high resistivity of polymers to form conductive channels that act as conduits for charge carriers generated due to interaction of radiations to reach the electrodes [75]. This phenomenon improves the charge collection efficiency (CCE) of the composite material as compared to the pristine material. Many papers have been reported to enhance the properties of the detector when polymers blend with MWCNT or composite with metals, semiconductors and clay [29].

Jose M. Lobez and Timothy M. Swager prepared a less expensive polymer (poly(olefin sulfone)/MWCNT blend and doped it with high-Z bismuth composite for the gamma rays detection. In this composite, the conducting MWCNTs dispersed in the polymer matrix form a percolated network which serves as conducting channels for charge collection [69]. Similar detection mechanism is also discernible in semiconductor-polymer composites which offer increased signal strength of detector. Investigations have been done on high-Z compound semiconductor CdTe quantum dots and their polymer nanocomposites for detection applications [27]. A.M.S. Galante et al. have performed studies on pre- and post-irradiation stability, samples were irradiated with 60-Co gamma radiation source, in free air at electronic equilibrium conditions, dose range between 1 and 150 kGy, and the results are indicative that fluoropolymers are very stable under different environmental conditions [76].

Intaniwet et al. have demonstrated that X-ray attenuation coefficient can also be increased by adding high-Z material (like Bi_2O_3) nanoparticles to a semiconducting polymer (polytriarylamine) (PTAA)). When samples with PTAA device containing 60 wt.% Bi_2O_3 nanoparticles are irradiated with 17.5 keV X-ray beams, sensitivity of detector upsurges approximately 2.5 times compared to the plain PTAA sensor [77]. Shruti Nambiar et al. prepared lead-free, polydimethylsiloxane (PDMS) nanocomposites incorporating varying weight percentages (wt.%) of bismuth oxide (BO) nanopowder and studied their affectiveness for shielding against diagnostic X-rays. Their study revealed that the PDMS/BO nanocomposite (44.44 wt.% of BO and 3.73 mm thick) was affective for attenuating all the scattered 60 ksVp X-rays, usually used in IVR [78]. A flexible metal–oxide Bi_2O_3 nanoparticle detector has also been fabricated for X-ray sensor device affirming the scope of high-Z-polymer composites for fabrication of flexible detector devices [79].

These fascinating results show that polymer composites with high-Z materials and/or conducting filler like CNTs are latest, novel high-performance materials for developing radiation detectors with high stability, better environmental conditions, high sensitivity and attenuation coefficient [80]. After a comprehensive discussion on the performance metrics and limitations (Table 2) of the different classes of semiconductor detector materials, further, in this review paper, our discussion shall be focussed on the potential and limitations of BiI_3 in context of radiation detectors.

BiI_3: a potential non-toxic RTSD

Bismuth (Bi) is the highest non-radioactive material which makes the material another high-Z material like good substitute of lead-, mercury- and cadmium-based detector devices with better performance and low toxicity. The potential use of this material as radiation detector was introduced in 1995 by Keller et al. through investigations of properties of BiI_3 crystals grown by physical vapour transport method [81]. Despite good resistivity as reported in their work, no response to α-particles or gamma rays was observed in the experiment due to high leakage current and inherent traps in material because of impurities. In 1999, Dmitriyev et al. [82] explored the optical and electronic properties of the material for prospective radiation sensing applications. However, in 2001, Matsumoto et al. were the first ones to report the detection of α-particles by BiI_3-based nuclear radiation detector [83]. Later, in 2014, Garg et al. reported the synthesis of thin films of bismuth tri-iodide using thermal vaporization technique and reported high value of resistivity [84]. Since then, there has been tremendous ongoing research work focused on BiI_3 semiconductor and its development as a room-temperature semiconductor radiation detector [82, 85–88].

Structural properties and inherent defects of BiI_3

BiI_3 is a high-Z (Bi:83, I:53), layered compound semiconductor having rhombohedral crystal structure where the Bi^{3+} ions occupied 2/3rd octahedral site and the rest 1/3rd site is vacant in material, as shown in Fig. 3 [89, 90]. The layered structure of BiI_3 crystal has hexagonal sheets of I–Bi–I layers in A-B-C-A-B-C manner [91] with each Bi atoms at the centre of an octahedron of iodine ions and the Bi–I together bind with a strong covalent bond [92, 93]. The soft layered material exhibits anisotropy in its optical, mechanical and magnetic properties and is predisposed to plastic deformation due to its low mechanical strength [20]. Due to the anisotropy between the (001) and (010/100) planes, the

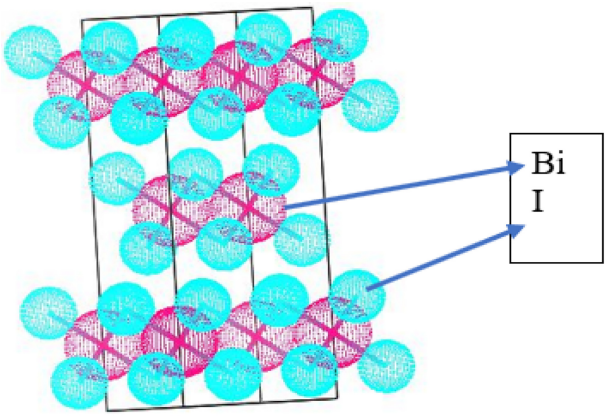

Fig. 3 Unit cell of BiI_3. The layers bond to each other with weak van der Waals forces. The Bi occupied 2/3rd site and the rest 1/3rd is vacant which acts as defects and traps

Table 2 Advantages and disadvantages of three categories of semiconductor detectors

Type	Advantages	Dis-advantages
Pure detectors	High carrier mobility	Low resolution for gamma rays
	Developed technology (Si and Ge detectors)	Required cryogenic system for cooling
	No dopants required	Expensive (diamond)
Compound detectors	High atomic number and density which makes them suitable for room-temperature operation	Low signal-to-noise ratio
	No need of cryogenic system for cooling as band gap lies in range of room-temperature operation	Toxicity
	Better resolution for high energies	Polarization with time
		Difficult to grow pure crystals
Polymer-high-Z composite detectors	Flexible and handheld devices	Plastic waste
	Low weight	Polarization
	Low cost	Need of conducting filler
	Recyclable	

mechanical strength shown by the lattice structure is dependent on the orientation of the measurement with the (001) planes of the crystal being cleaved off with ease, while the rigid (010) and (100) planes exhibit higher yield strength. Also, for the weak bonding between I–I layers there are lattice vacancies and stacking disorder between BiI_3 crystal planes [94]. Stacking faults in BiI_3 and polytypes results from deviation in the repeated stacking pattern of I and Bi in their planes form a new direct band gap transition replacing the normally indirect transition, giving rise to the P defect energy level [95].

This discrepancy may be attributed to the presence of polytypism [63], defect and trap states within the crystal structure and the inherent structural voids as potent sites for impurity atoms arising due to layered structure of BiI_3 [96].

The inherent defects can lead to introduction of shallow or deep level defect states in the band structure of BiI_3. These defects in BiI_3 crystal act as trap states for the charge carriers generated by radiation photons leading to reduction in the signal strength and SNR of detector, affecting the quality of detector reducing its ability to generate gamma ray spectra with good resolution [46, 97].

Oxidation of material is another problem with BiI_3 [98]. At higher temperature, the Bi^5 and I_2 reacted with water to form Bi_5O_7I, BiOI and Bi_2O_3. BiOI is the main product of hydrolysis in environment, although placing the samples in some inert gas and dry ice can intact the material [99]. The deterioration in the generated photocurrent response spectra owing to the presence of point or microstructural defects in the detector is abridged by research in polymer-based BiI_3 composites recently [73, 79, 100]. Energy resolution of a detector depends on its photon stopping power which increases with density and atomic number of materials (Fig. 4).

For the energy range 10–100 keV photoelectric affect is the most desired interaction of the material which depends on the attenuation coefficient [101] of a material varies as Z^x ($x=4$ or 5) and further the interaction probability between incident radiation and material depends both on the attenuation coefficient and the incident radiation energy (E^{-3}). Owing to the high-Z, the attenuation coefficient of BiI_3 is high, making it a potential candidate for medical and security applications in the range of 10–100 keV [102, 103]. The intrinsic photopeak efficiency of BiI_3 is not the highest amongst other semiconductor detectors like Hg- and Cd-based detectors, but less toxicity of BiI_3 makes it relatively easy to grow crystal and handle [104].

Electronic properties of BiI_3

Electronic properties like resistivity, mobility-lifetime product and transportation properties of charge carriers play an important role in investigations of BiI_3 as a material for

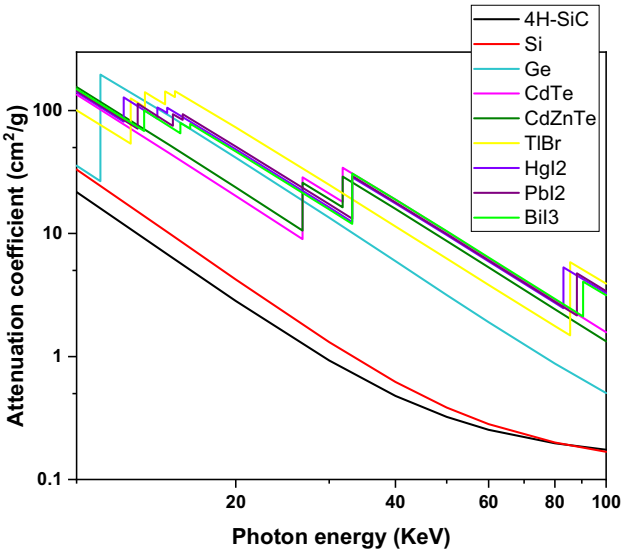

Fig. 4 Total linear attenuation scattering cross section (without coherent scattering) for various available detector materials with low radiation energy range 10–100 keV. Data are calculated from NIST XCOM Database

RTSD [82]. The electronic properties are strongly prejudiced by the band gap of the material, it has been reported that an indirect transition between the A and Γ conduction band points, and the Λ and A valence band points produced by the lowest energy gap between valence and conduction bands in BiI_3 give band gap of 1.67 ± 0.09 eV [105]. Also, the potential barrier associated with various inhomogeneities of structural crystal defects (deep or shallow defects) affected the carrier collection and transport kinetics of material [106]. The electrode configuration and material of electrode deposition are also strongly affecting the charge collection. Particle size and density get affected by thickness of detector which impact mechanical properties of film or pallet [107]. Resistivity of a material may vary with different synthesis techniques leading to a wide range of detector parameters. Table 3 presents the various parameters of BiI_3 deposited with different techniques and with different thickness, which tailor the required properties of the material to be a potential radiation detector.

It is also observed that the resistivity and charge carrier collection in a semiconductor vary drastically with electrode material, its configuration and the type of contact, i.e. Ohmic or Schottky. Three types of electrode configurations reported by Yizhen Liu et al.: planar or parallel (Electric Field, *E* is parallel to *c*-axis), perpendicular (*E* perpendicular to *c*-axis) and co-planar with Au electrodes or Pd electrodes, are depicted in Fig. 5 [122].

Liu et al. [122] analysed the internal distribution of electric field within the BiI_3 detector using different configurations of electrodes and reported dependence in photocurrent

Table 3 The electronic properties of BiI_3 in detecting high-energy radiations of different energies synthesized under different growth conditions:

Detector material/growth technique	Resistivity (Ohm-cm)	Thickness	Source energy/dose rate	Conclusion	References
BiI_3/PVD	1.7×10^{13}	50–80 µm	Am-241 (59.5 keV)/3.5 mR/h	Sensitivity: 4940 µc/Rcm^2; bias: 60 V; SNR: 11	[108]
BiI_3/Theoretical work				For 662 keV energy source BiI_3 has intrinsic photo-peak efficiency of 19%	[109]
BiI_3 layered on HgI_2/particle-in-binder method	5×10^9	250µm (double layer)	X-rays (70kVp)	Electric field: 1 V/ µm; Sensitivity: 15 nC/mR/cm^2	[110]
BiOI film on BiI_3/Thermal evaporation	10^{11}	2-50µm	X-rays (70kVp)	Sensitivity:0.8(pc/cm^2)/(nc/kg) (thickness 15 µm) at 0.2 V/µm and for thickness 4µm, 1.3(pc/cm^2)/(nc/kg) at 5 V/µm. Response time: 33 ms	[111]
BiI_3/PVD/TMZ	2×10^{12}	50–80 µm	Am-241 (59.5 keV)/3.5 mR/h	Sensitivity: 8230 µc/Rcm^2 at 30 V bias voltage; SNR: 5.1	[112]
BiI_3/PVD	1.4×10^{13}	5–60 µm	X-rays (40kVp)/2.7 R/min	Dark current density: 9.7 pA/mm^2 for 5.6 V/µm; $\mu t = 3\times10^{-7}$ cm^2/V; S/N is 2.3; sensitivity: 23 nC/R cm^2 at 1 V/µm	[113]
BiI_3 nanostructures/hydrothermal method	10^{11}	20 nm	Am-241 (59.5 keV)/3.5 mR/h		[114]
BiI_3		$5\times5\times10$ mm^3 volume	Gamma ray	mobility-lifetime product for electrons and holes were 9.5×10^{-6} and 1.0×10^{-7} cm^2/v, calculated by Modified Hecht Equation	[115]
BiI_3/PVT	2.27×10^{10}	0.926 cm	Am (241)	FWHM recorded for energy 5.48 V was 1.46 eV, bias voltage 250 V; mobility (e): 433 ± 70 cm^2/V; pulse response time: 200 ns	[116]
Sb-doped BiI_3/Vertical Bridgman	2.6×10^9	0.4 cm	Am alpha	Resolution: 62.66% and 32.96% after 5 min and 8 h at 213 V bias voltage; Leakage current density: 10^{-2}µA/cm^2; Response time: 881.8 ns	[117]
BiI_3/Modified Bridgman	10^8–10^9	0.42 mm	Alpha source	Mobility(e): 260 ± 50 cm^2/Vs at bias 50 V; electric field 1190v/cm; signal recorded weaker than expectation < 1 mV	[118]
Sb-doped BiI_3/vertical Bridgman		0.68 cm	Gamma ray and Am-241	Resolution observed 2.2% for 662 keV and 4.5% for 59.5 keV at voltage 2630 V/cm	[86]
Sb/BiI_3/Bridgman method	3.4×10^9			Improvement in FWHM obtained by XRD by 349%	[87]
Sb/BiI_3/Modified vertical Bridgman		0.5 and 0.2 cm	Gamma ray	7.5% energy resolution at 0.5 cm at bias voltage 118 V; 9.35% at 0.2 cm at bias voltage 185 V for 59.5 keV; µt (electron): 5.2×10^{-4} cm^2/V	[119]
BiI_3/ PVT	1.6×10^{11}	100 µm	22 and 59.5 keV	Resolution for energy 22 keV recorded 61% and for 59.5kev was 29% at bias 10 V using amplifier. CCE: 60%; electron–hole pair creation energy: 5.8 eV; µt(e): 1.6×10^{-6} cm^2/V	[59]
BiI_3 single-crystal flakes/ PVT	5.8–6.4×10^{11}	10–100 µm	X-ray (60KVp)	Sensitivity: 1.22–1.36×10^4µc/Gy/cm^2; Bias voltage 50 V; band gap: 1.75 eV; Response time: 0.08–0.11 s; Recovery time: 0.09–0.12 s	[120]
BiOI and Bi_5O_7I/nanocrystals		146 and 165 µm	X-ray (70 kVp)/ 7.97 mGy	2 V bias voltage, Sensitivity: 1.926 (BiOI) and 1.318(Bi_5O_7I) nC/mGycm^3; Band gap: 1.7 (BiOI) and 3.2 (Bi_5O_7I) V. SNR: (0.02)	[121]

Table 3 (continued)

Detector material/growth technique	Resistivity (Ohm-cm)	Thickness	Source energy/dose rate	Conclusion	References
BiI_3/PVT	3.50×10^{13}	80–120 µm	X-ray(60kVp)/ 489.78 µGy/h	Sensitivity: 0.526×10^{4}µc/Gy/cm^2 at 0.02 V/µm; SNR: 896.4; rise time: 0.3; fall time: 0.32	[122]
BiI_3-PS composite/Dry-tumble Technique	10^{10}	1 mm	X-ray (30 kVp)	SNR: 70 at 50 biases; dark current density: 10^{-11} A/cm^2; Response/recovery time: 0.3/0.35 s	[123]

intensity on the three electrode configurations because of anisotropic nature of the lattice structure. In the case of *E* parallel to *c*-axis configuration, layer-to-layer transport of charge carriers results in low photocurrent owing to the fact that the photo-generated charge carriers are scattered or trapped by the defects congregated between I–Bi–I layers, thus influencing the number of carriers that drift through layers to reach the electrodes [124]. In case of co-planar configuration, this layer-to-layer charge carrier transport builds up an interlayer interface scattering below the electrode which collects the carriers and, thus, lowers the photocurrent. But, in $E\perp c$-axis configuration, the influence of trapping affect to transport carriers along the *c*-axis can partly be reduced when the electric field is applied. The photo-induced carriers drift along (00 l) plane where they are generated and then collected by electrodes on (110) plane. This mode of transportation of charge carriers reduces scattering and trapping affect which leads to the high photocurrent than the other two configurations.

The relation of resistivity and dark current for BiI_3 with different electrode configurations as reported in the literature over the past more than two decades are represented in Table 4 and Fig. 6. A comparison of results of gold-coated glass substrate reported by Aguiar et al. for the resistivity and dark current values reported for gold and palladium electrodes with uncoated glass substrate by Fornaro et al [108] indicate gold-coated glass substrate as a clear winner.

Also, Fornaro deposited Pd electrodes on as-grown platelets with and without ring guard and reported that the quality of detector was enhanced owing to better resistivity and low dark current value with Pd wire ring guard than without ring guard [108]. The ring guard arrangement is depicted in Fig. 7 with the rings deposited on both sides of sensing electrodes with an insulating gap between them.

This configuration increases the bulk resistivity of detector by 20–40% which leads to decrement in dark current as compared to the configuration without ring guard [125]. Also, the electric field lines are uniform in ring guard configuration which results in increase in charge collection on electrodes. The comparative data in Table 4 show that best resistivity is demonstrated with parallel gold electrode configuration by Yizhen Liu et al. [122]

Mobility-lifetime product

Mobility-lifetime product ($\mu\tau$) for charge carriers is one the most important property which decides the charge collection within detector. Ideally µτ of material should be high enough to reach electrodes before getting trapped into a trap or recombination centre. BiI_3 is a layered compound semiconductor, having trap states or defects in the material. These impurities, dopants and defects within the semiconductor acts as recombination centres and results polarization

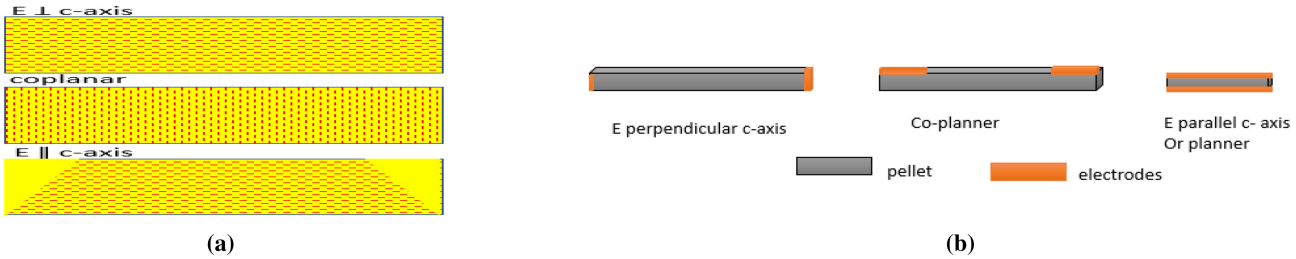

Fig. 5 Three-electrode configuration **a** $E \perp c$-axis, co-planer and planer. Electric field lines for all configurations are represented in Fig. 5(a) and charge carrier transport **b** represents electrode deposition. The CCE is maximum for E⊥c-axis configuration

Table 4 Variation of resistivity and dark current of BiI_3 detectors with a different electrode configuration/type and material used. Also, substrate coated with gold shows better results than glass or ITO substrate

S.no	Resistivity (10^{11} Ω-cm)	Dark current (pA/mm^2)	Electrode type/ configuration and material used	References
1	2.82		Co-planner	[122]
2	350	0.5	Parallel	[122]
3	3.43	2.1	Perpendicular	[122]
4	170	46	Ring guard with electrode	[108]
5	26	324	Electrodes without ring guard	[108]
6	20	55	Gold (PVD)	[112]
7	15	140	Palladium (TMZ)	[112]
8	14	420	Palladium (PVD)	[112]
9	140	20.6	Gold coated substrate	[113]

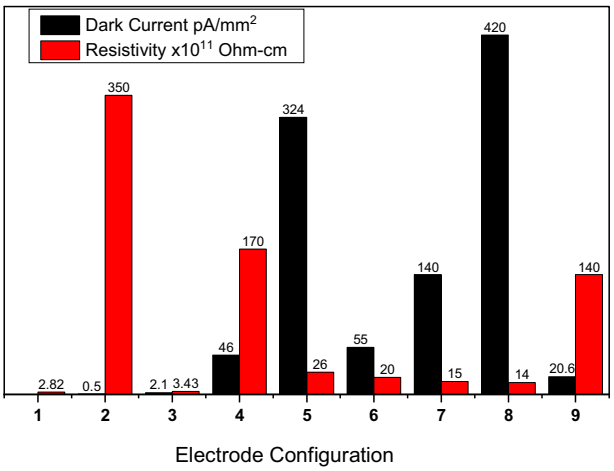

Fig. 6 Variation of resistivity and dark current of BiI_3 detectors with different electrode configurations and types. The resistivity of detector (Red) should have higher values, and leakage current (Black) should be lower. The electrode configuration or type on Y-axis is given in Table 4. The highest difference between black and red dot gives best result

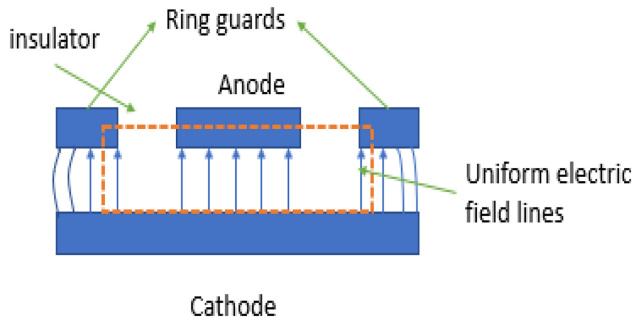

Fig. 7 Guard-ring electrode configuration with uniform electric field lines. The guard rings are at same voltage as the charge collection area (anode). The uniform electric field increases the resistivity of detector

and low SNR. The defects (deep or shallow) also play major role in charge carrier transportation (Fig. 8). BiI_3 undergoes a transient current peak phenomenon which can be observed when a reversal voltage is applied to the detector just before carrying out the leakage current measurement as reported by several researchers including Han et al. [117] and Gokhale et al. [119]. This transient peak arises due to the slow de-trapping of holes when they drift towards cathode electrode. This affect can interfere with the signal generation due to photocurrent carriers as drifting space charge is created by these de-trapping of holes. To reduce this affect or resolve transient current, BiI_3 must be given sufficient time and high mobility to achieve thermal equilibrium before the photocurrent spectra can be attained.

The mobility-lifetime ($\mu\tau$) product for charge carriers, i.e. electrons and holes, is usually calculated from the amount

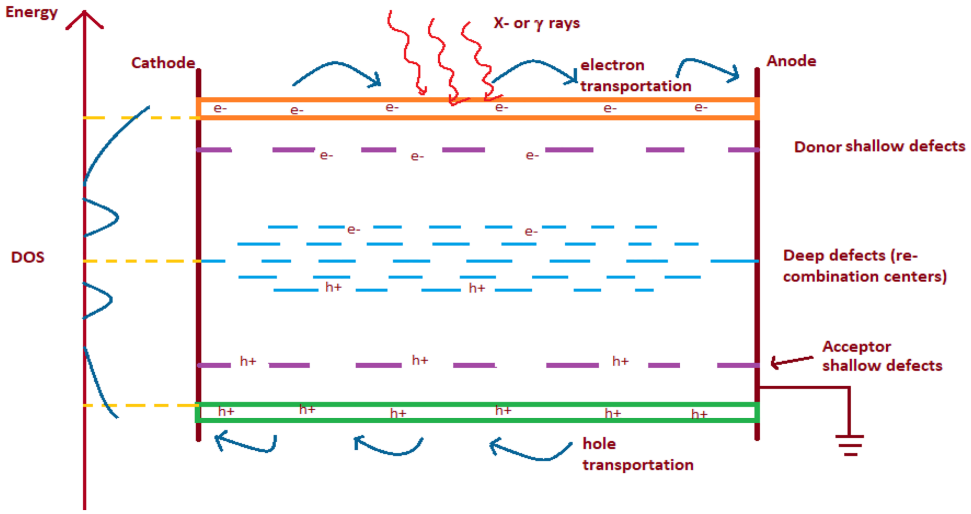

Fig. 8 Incident radiation on detector generates electron–hole pair in device which drift towards respective electrodes. The defects (deep and shallow) in the path of two electrodes traps these charge carriers. Thus, these defects act as recombination centres for the charge carriers

of induced charge, Q, by the Hecht equation [126], given by the relation 1:

$$Q = N_0 q \frac{\mu_e \tau_e V}{D^2}\left[1 - \exp\left(\frac{-D^2}{\mu_e \tau_e V}\right)\right] \quad (1)$$

$$\text{CCE} = \frac{Q}{N_0 q} = \frac{\mu_e \tau_e V}{D^2}\left[1 - \exp\left(\frac{-D^2}{\mu_e \tau_e V}\right)\right] \quad (2)$$

where N_0 is the density of charge carriers generated on ionization, q is the elementary charge, V denotes bias voltage, and D is the detector thickness. The charge collection efficiency (CCE) of detector at the minimum operating bias voltage [20, 126] is expressed in Eq. (2), [127]. Enhancement of CCE of a detector requires either a decrease in the detector thickness or an improvement in the μτ of the material. Thus, the electronic and charge transportation properties of BiI_3 are interrelated and strongly bias by operating voltage, crystal structure, inherent defects or impurities, trap states and phonon interactions [13] which can be tailored by restraining control over synthesis parameters of the material. By tuning these properties through material engineering, the performance of the detector can be enhanced. Dmitriyev et al. first reported the value of $\mu\tau$ for e–h pairs in BiI_3 as 9.5×10^{-6} cm^2/V for electrons, and almost undetectable, i.e. below 10^{-7} cm^2/V for holes using excitation wavelength of 450 nm at 100 V bias voltage. The crystal grows polycrystalline and single-crystal cleavage in (0001) of thickness 0.4 mm [82]. Paul M. Johns in his work has confirmed that for BiI_3 $\mu\tau$ values may be improved up to an order hundreds cm^2/V-s for electrons or holes [20].

Table 5 conclusively indicates that as the thickness of polycrystalline detector sample increases, the mobility lifetime of the electron decreases as transit time for charge carriers overcomes the lifetime of charge carrier and thus the probability of recombination increases. In case of single crystal, the impurities and thus the trap states in samples decrease thereby resulting in an increase in μτ. The mobility lifetime of the electron can further be augmented by subjecting the material to purification through zone refining [59, 118]. Gokhale et al. have adopted purification of material through multiple zone passes for synthesis of ultra-pure material and reported that the μτ for the sample increases for samples with thickness of even as large as 1 mm [116].

Table 5 Mobility-lifetime product reported of different thickness and crystallinity of detector

S. No	$\mu\tau$ (electron) (cm^2/V)	Thickness	Bias voltage (V)	Crystallinity	Source energy	References
1	3.4×10^{-6}	30 μm	15	Polycrystalline	Am-241 (59.5 keV)	[59]
2	3×10^{-7}	50 μm	300	Polycrystalline	X-ray (40 kVp)	[113]
3	10^{-6}	130 μm	50	Polycrystalline		[128]
4	260 ± 50	0.71 mm	70	Single crystal	5.48 MeV	[118]
5	400	0.9 mm	250	Single crystal (ultra-pure)	5.48 MeV	[116]
6	9.5×10^{-6}	5 mm	100	Single-crystal cleavage from Polycrystalline ingot	450 nm	[82]

The defects of detector affect by impurities in the material which are affected by crystallinity (synthesis process)

Also, at high electric field the charge carriers are able to overcome the shallow defects in material, but deep defects in semiconductor trap the charge carriers and became recombination centres.

The Hecht equation (Eq. 1) can often predict unreliable ($\mu\tau$) product due to limitations of the technique when surface damage, ballistic deficit, or perturbations in the weighing potential are present in a detector. A geometry correction factor '*k*' is calculated by detector thickness to avoid the error [129].

Sensitivity and response/recovery time

Sensitivity is a crucial parameter for detector's performance that gets governed by signal and noise levels [130]. Sensitivity of a radiation detector is measured by the relation 3:

$$S = \frac{\int \left[I_{\mathrm{p}}(t) - I\right] \mathrm{d}t}{D \times V} \tag{3}$$

where I_{p} is photon current, I is dark or leakage current of detector, D is radiation dose and V denotes volume of detector. Thus, the sensitivity of any detector depends on difference of signal and noise as depicted by photocurrent and dark current, respectively, and on cross section of a given detector and can be modified by various parameters like incident radiation, resistivity of the material, bias voltage and thickness of the detector. Sensitivity for BiI_3 is reported by many researchers as summarized in Table 6, for different radiations and at different bias voltages.

The response and recovery time for a detector is an important parameter to decide the device performance in real-time applications. It is defined as the time taken by the detector to reach 90% of response or recover to original state, when a radiation interacts with the device in a definite interval of time (shown in Fig. 9).

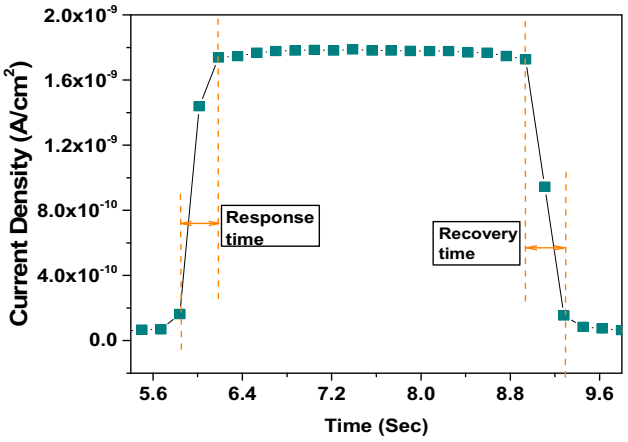

Fig. 9 Response time and recovery time calculation from radiation response. The response/recovery time of any detector is calculated by the response graph. When radiation is incident on the detector, it generates photocurrent which is shown in Fig. 10, the time period requires to record the photocurrent can calculate from the response graph

Generally, the reported response and recovery time for X-ray detector is less that one second (Table 6) and it is also considered a significant time for device fabrication. Aguiar et al. initially record the response of X-ray (40 kVp) for polycrystalline BiI_3 films at 50 V and the sensitivity of detector was 2.6 μC/Gy-cm^2 [113]. This value of sensitivity though was not remarkable for device applications, nonetheless gave a substantial lead about the potential of BiI_3 for X-ray sensing applications. Ikeda et al. deposited a blocking layer of Bismuth oxy-iodide (BiOI) (*p*-type) on the film of BiI_3 (*n*-type) in order to enhance the properties of detector by forming *p*–*n* junction [111]. The resistivity of detector increased from 10^9 to 10^{11}Ω-cm, thereby diminishing the dark current of device. The sensitivity was recorded 23.53 μC/Gy-cm^2 for thickness of 15 μm at 3V. The best result of sensitivity (38.24 μC/Gy-cm^2) was obtained by decreasing

Table 6 Sensitivity, SNR and response/recover time of BiI_3 detector. These parameters are strongly influenced by source radiation, resistivity, geometry of detector and the bias voltage

S. no	Sensitivity (μC/Gy-cm^2)	S/N	Response/recovery time (Second)	Resistivity (Ω-cm)	Radiation energy	Thickness (μm)/ area (cm^2)	Bias voltage (V)	References
1	2.6	2.3			X-ray (40KVp)	60/0.25	50	[113]
2	23.53		0.33/–	10^{11}	X-ray (70KVp)	15	3	[111]
3	38.24		0.33/–	10^{11}	X-ray (70KVp)	4	20	[111]
4	0.5×10^4	896	0.15–0.57/0.30–0.32	10^{13}	X-ray (60KVp)	100	2	[122]
5	1.3×10^4		0.08–0.11/0.09–0.11	10^{11}	X-ray (60KVp)	100	50	[120]
6	56.12×10^4	11		10^{13}	Am-241 (59.5 keV)	60/0.071	60	[108]
7	93.5×10^4	5.1		10^{12}	Am-241 (59.5 keV)	80/0.02	30	[112]
8	23.64×10^4	1.8		10^{11}	Am-241 (59.5 keV)	80/0.12	30	[112]
9	2.6				X-ray (70KVp)	200	2	[131]

the thickness of device to 4 μm at 20 V. Sun et al. deposited free standing single crystals along (001) plane on BiI_3 to reduce the impurity in material and further optimized the electrode configuration in order to get good results [120]. The sensitivity was recorded 1.3×10^4 and 0.5×10^4 μC/Gy-cm^2 for planar and co-planar electrode configurations at X-ray (60 kVp). Ring guard electrode configuration also increases the sensitivity and SNR as electric field lines are more uniform in this configuration (Fig. 7). Sensitivity of 93.5×10^4μC/Gy-cm^2 is obtained for Am-241 radiation by Fornaro et al. at 30V with gold electrodes on zone refined BiI_3 platelets [112]. Recently, Karthieka et al. deposited thick nanocrystalline BiI_3 films on wet-etch-derived interdigitated electrodes by glass rod sliding technique and the material displayed good sensitivity for low-dose X-rays at low bias (2 V) [131].

Also, a direct printable X-ray detector is fabricated using a straightforward digital printing process by micro-pyramid triclinic Bismuth Oxide (ω-Bi_2O_3) ink. The device showed sensitivity of 3.077 μC/Gy-cm^2 for low detection limit (56.95 $\mu Gy_{air} s^{-1}$) at bias 20 V and stable response to exposure of doses 5120 $mGy_{air} s^{-1}$ at ambient conditions for eight months [132].

Signal-to-noise (SNR) ratio

The limit of detection (LoD) is classified as the lowest dose limit the detector device can measure and is defined as IUPAC description labels as the minimum radiation that provides an SNR = 3 [133]. The SNR is given by Eq. (4). It is the ratio of photocurrent to the maximum error or fluctuations in the photocurrent, i.e. calculated by standard deviation in photocurrent by the recorded response spectra. The high value of SNR leads to better imaging quality of the detector.

$$\mathrm{SNR} = \frac{I_\mathrm{P} - I_\mathrm{d}}{\sqrt{\frac{1}{N}\Sigma_i^N \left(I_\mathrm{i} - I_\mathrm{P}\right)^2}} \tag{4}$$

I_p is photocurrent, I_d is dark current, and the denominator represents a standard deviation in photocurrent at fixed bias voltage. The SNR value of the detector is mainly dependent on energy of the incident radiation, bias voltage of detector, crystal lattice of detector material and trap states.

It can be observed from Fig. 10 that at low voltages the value of SNR for X-rays is less perceptible. Praveen Kumar et al. explored the possibility of nanocrystalline bismuth oxyiodides for the low-dose X-ray detectors but the SNR calculated from that work is very low (0.02) at 2 V. At low bias voltage, the generated carriers possess insufficient kinetic energy to reach electrodes thus the difference between photocurrent and leakage current is trivial. In Fig. 10, SNR ratio

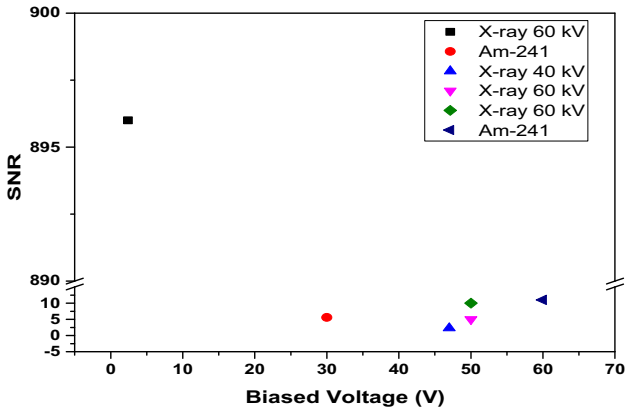

Fig. 10 The graph shown reported values of SNR by different groups for different values of incident radiation. The y-axis represents the SNR ratio, and the break in axis is to signify the whole range

for BiI_3-based detector exposed to X-rays (60 kVp) reported by Liu et al. is highest. They controlled the resistivity of detector by changing electrode configuration (parallel, planar and co-planar) (Fig. 6) and got minimum leakage current and maximum signal current, i.e. highest SNR ratio.

Recent development in BiI_3

Polymer-high-Z matrix is explored by many researchers, and the results are a strong indication of improved sensitivity and better image quality for portable devices. Cherepy et al. have investigated the properties of transparent composite materials, single-crystal SrI_2(Eu), GYGAG(Ce) and bismuth-loaded plastics for gamma ray spectroscopy applications and have reported energy resolution of 2.7% at 662 keV with SrI_2(Eu), 4.5% with GYGAG(Ce) crystals and 9% at 662 keV with bismuth-loaded plastic detector. GLO(Eu) offers high light yield of 70,000 photons/MeV, high stopping potential and low radiation damage rendering it as an excellent material for detectors. These Bi-loaded plastics are an advanced class of materials used in designing scintillator-based detectors [134]. Transport of charge carriers is extremely sensitive to the properties of the semiconductor/dielectric interface [135]. Due to the resistivity difference between polymer and semiconductor material, the semiconductor material acts as conductive tips in polymer matrix to improve the transport mechanism (Fig. 11) [136].

Our group is working on the BiI_3-polymer composites for applications in direct X-ray imaging devices at low-dose rate. Chaudhari et al. have prepared BiI_3-Polystyrene composite pellets of thickness 1 mm and studied the response for low X-rays energy (30 kV) at 13 V bias. The XRD and IV studies shows better structural and electronic properties than pure BiI_3 pallets. The composite enables a good charge collection efficiency even at low bias voltage of 13 V. The

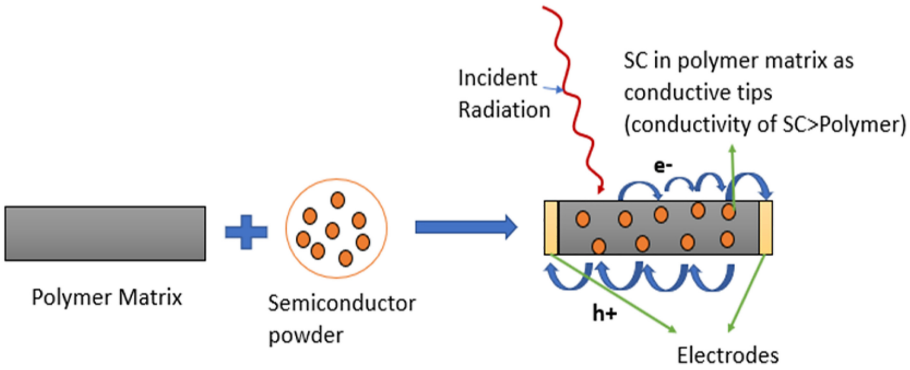

Fig. 11 The semiconductor (SC) in polymer matrix acts as conductive tips. High electric field on these tips increases the drift velocity of generated charge carries and provides a path to electrodes which enhanced the CCE of detector

signal-to-noise ratio is calculated from switching graph for sample with 50:50 weight % ratios if BiI_3 and polymer at 50 V is fairly high at 70. As the bias voltage was increased beyond 50 V, dark current increased due to thermal excitation of electrons and interfere with signal collection at the electrodes. The sensitivity achieved for PS-50 (sample with 50:50 weight % ratios if BiI_3 and Polystyrene) was 189 μC Gy^{-1} cm^{-3} which is nine times better than the commercially available α-Se detectors (20 μC Gy^{-1} cm^{-2}). Also, the SNR, 3300 demonstrated by the polystyrene-BiI_3 composite. The response and recovery time of the detector is fast around 30 ms [123, 137]. Further on incorporation carbon filler within the polymer composite sample collected up to 93% of charge carriers at a low bias of 0.8 V for 60 kV X-rays source. The elimination of charge trapping within the sample by adding conductive fillers can be a better and efficient way to enhance the CCE and photocurrent in the direct X-ray detectors. Amorphous nature of polystyrene has superstructure of fillers segregate in amorphous region which increases the filler contact resistance resulting in high threshold which helps in suppression of dark current. An interesting phenomenon here is that these segregated fillers have a separation distance that favours tunnelling/hopping affect for the X-ray induced charge carriers leading to enhancement of the photocurrent in the detector [138]. This improves the overall SNR of the sample by keeping the noise in limits. This leads to better sensitivity, high SNR and low NED for the detector [139]. Also, the prepared polymer matrix composite samples results indicate high defect tolerance, high mobility-lifetime, low noise and a sensitivity of 0.6×10^3 μC/Gy-cm^3 against dose rate of 500 μ-Gy/sec. at 30 V bias for 60 kV X-rays. The stability investigations of sample demonstrates that the composite offers great stability in terms of both reproducibility and repeatability in ambient environmental conditions under strong radiation dose, even after one month of exposure. After continuous testing for 35 days, composite pellet detector maintains a stable response with less than 10% decay.

Addition of fillers in composites like CNT, graphene etc. leads to improve the molecular interaction in composite matrix to boost the performance of the new polymer composite for detector applications [73, 80]. Overall, the composite maintains high resistivity with improved mobility-lifetime and charge collection efficiency.

Ultrasensitive X-ray detector is fabricated by Xiaojia Zheng et al. using zero-dimensional (0D) methylammonium bismuth iodide perovskite ($MA_3Bi_2I_9$) single crystals as activation energy for charge carriers migration is high in Zero-dimension. The detectors show sensitivity of 10,620 μC/Gycm^2 to doses of 0.62 nGy s^{-1} and have no degradation in performance was observed in sensing of a dose of ~ 23,800 mGy which is comparable to > 200,000 times the dose required for a single X-ray chest radiograph in hospitals [140].

Summary and future scope

The review is focused on semiconductor detectors wherein direct conversion of photon energy to signal offers better response spectra with high resolution, sensitivity and SNR than gas and scintillation detectors. The latest advancements in the semiconductor materials for radiation detector applications have been elaborated in the manuscript. The use of semiconductor detectors can bring significant development in the field of radiation detection and dosimetry. However, the challenge is to choose a suitable non-toxic semiconductor material and subsequently engineer the material properties and device architecture for radiation detectors.

A. Much effort has been made to develop wide band gap, high-Z semiconductor materials for room-temperature radiation detection. CdTe, CZT, TlBr, HgI_2 PbI_2 are considered the most explored, and promising materials are fulfilling various scientific parameters and performance metrics required for a room-temperature radiation detector. However, their selection as an ideal material for RTSD has also been constrained by several demerits such as polarization affects due to high bias voltage, poor control on trap states, etc. Toxicity associated

with using Hg-, Cd- and Pb-based compounds is another excellent matter of concern. Despite the significant progress made in semiconductor materials for radiation detector applications, many problems and unprecedented challenges still need to be overcome to improve further the detection performance of these materials for their practical applications.

B. *Driven promising material* After an elaborative review of many compound semiconductor materials for detector applications, authors conclude BiI_3 to be a potential, non-toxic promising candidate for RTSD. But the presence of trap states in the bulk samples that act as recombination centres for the generated charge carriers are the significant limitations reported in BiI_3 detectors. The defects in bulk structure led to polarization in detectors under high bias voltage after extended usage. Thus, tailoring defects and trap states in the material is of paramount importance and optimization of various electrode configuration designs has led to improvement in the CCE of the detector resulting in a high SNR and sensitivity. However, the synthesis of large volume (several mm^3 to cm^3), defect-free, high purity BiI_3 single crystals required for high-resolution detector fabrication is a tedious and complex process involving heating, purification and growth. These challenges still need to be addressed to level up the research to device fabrication.

C. *Technological Advancements* Various technological advancements in material synthesis and detector fabrication have been made to overcome the above-mentioned constraints. BiI_3-based composites and perovskites are now being used to achieve enhanced detector performance, and these materials have shown excellent results as direct X-ray detectors. Perovskites single crystals can be grown to several cm^3 successfully, but their electronic instability is a significant issue to be resolved. To achieve high SNR at low bias voltage, incorporating conductive fillers like CNT (carbon nanotubes), rGO (reduce graphene oxide), etc., in polymer matrix incorporated with high-Z material like BiI_3 can be a way for future technology. The conductive fillers assist the hopping of charge carriers to the electrodes before getting trapped into the defects, increasing the device's CCE even at low bias voltage. Low-voltage operation reduces the cost of device fabrication and also lowers the polarization affect in the material. This increases the longevity of the detector device. However, a diligent trade-off is to be maintained in the amount of these fillers added, as it may increase the leakage current, thereby deteriorating the SNR and resolution of the device. BiI_3 composites may thus find potential prospects in applications like medical and security areas when there is a need for lightweight, portable handheld detector devices capable of low bias and room-temperature operation.

Conclusion

Portable and handheld flat panel direct X-ray detector devices are need of the hour for future medical and security applications. Pb- and Cd-based semiconductors grab a major niche in the market of X-ray detectors. However, BiI_3 is currently emerging as a prospective candidate in the X-ray detector domain. High-Z semiconductor, BiI_3 stands out as a non-toxic candidate with high attenuation coefficient and resistivity that leads to better resolution, sensitivity and SNR. Flexible polymer BiI_3 composites offer great potential for development of flat panel detectors and can be investigated for portable and wearable X-ray detector devices. Further, BiI_3 polymer composites may find consequential applications in more challenging device integration such as the development of integrated PET–MRI (Positron emission tomography–magnetic resonance imaging) devices, where the PET detector is placed inside the high magnetic field of the MRI system making the use of conventional photomultiplier tubes impossible. High-Z semiconductor materials such as BiI_3 will continue to play a central role in developing advanced radiation detectors for years to come. Further advancement in detector technologies will be driven by considering novel perovskite composites and design of innovative architectures to confer enhanced detector performance.

Acknowledgements RC acknowledges Indira Gandhi Delhi Technical University for Women for IGDTUW Senior Research Fellowship and various infrastructure and facilities for research.

Declarations

Conflict of interest Authors do not have any conflict of Interest.

References

1. A.M. Bagher, Advantages of gamma radiation in science and industry. J. Adv. Phys. **3**, 97 (2014)
2. F. Tabatabaei, More about radioactive pollution. Heal. Scope **1**, 99 (2012)
3. A. Vaiserman, A. Koliada, O. Zabuga, Y. Socol, Health impacts of low-dose ionizing radiation: current scientific debates and regulatory issues. Dose-Response **16**, 155932581879633 (2018)
4. K. Kamiya, K. Ozasa, S. Akiba, O. Niwa, K. Kodama, N. Takamura, E.K. Zaharieva, Y. Kimura, R. Wakeford, Long-term effects of radiation exposure on health. Lancet **386**, 469 (2015)
5. W. Lin, Q. Yi-min, H. Bo, Z. Zhi-ming, W. Xian-yong, C. Qing-ru, Z. Guo-lin, Study on the reaction mechanism of naphthalene with oxalyl chloride. Wuhan Univ. J. Nat. Sci. **6**, 854 (2001)
6. A. Kumar, *How Careless Dumping Of Radioactive Material In Delhi's Mayapuri Has Damaged Lives*, Youth Ki Aawaj (2016).
7. L. Wu, Y.M. Qin, B. Huang, Z.M. Zong, X.Y. Wei, Q.R. Chen, G.L. Zou, Study on the reaction mechanism of naphthalene with oxalyl chloride. Wuhan Univ. J. Nat. Sci. **6**, 854 (2001)

8. *Why Do We Need Radiation Detectors ?*, http://depts.washington.edu/imreslab/from old SITE/pet_intro/nmphysics_fall07/radiation_detection_Fall_2007.pdf.
9. S. Usman, A. Patil, Radiation detector deadtime and pile up: a review of the status of science. Nucl. Eng. Technol. **50**, 1006 (2018)
10. S.V. Chuklyaev, A.S. Koshelev, Gas-filled ionization chamber and secondary-emission detector for measuring γ-ray dose rate. At. Energy **128**, 166 (2020)
11. F. Zhou, Z. Li, W. Lan, Q. Wang, L. Ding, Z. Jin, Halide perovskite, a potential scintillator for X-ray detection. Small Methods **4**, 2000506 (2020)
12. K. Moshkbar-Bakhshayesh, Constructing energy spectrum of inorganic scintillator based on plastic scintillator by different Kernel functions of SVM learning algorithm and TSC data mapping. J. Instrum. **15**, P01028 (2020)
13. S. D'Auria, *Introduction to Radiation*, in (2018), pp. 1–11.
14. Mirion Technologies, Gamma and X-Ray Detection Detector Overview, 2014.
15. K. Kumar, P. Arun, C.R. Kant, N.C. Mehra, V. Mathew, The effect of cesium metal clusters on the optical properties of cesium iodide thin films. Appl. Phys. A Mater. Sci. Process. **99**, 305 (2010)
16. K. Kumar, P. Arun, C. Ravi Kant, N.C. Mehra, L. Makinistian, E.A. Albanesi, Effect of residual stress on the optical properties of CsCl thin films. J. Phys. Chem. Solids **71**, 163 (2010)
17. K. Kumar, P. Arun, C. Ravi Kant, B.K. Juluri, Metal cluster's effect on the optical properties of cesium bromide thin films. Appl. Phys. Lett. **100**, 2010 (2012)
18. A. Mirzaei, J. Soo, H. Sang, S. Kim, H. Woo, Room temperature hard radiation detectors based on solid state compound semiconductors : an overview. Electron. Mater. Lett. **14**, 261 (2018)
19. G. Lutz, in *Semiconductor Radiation Detectors* (Springer, Berlin Heidelberg, Berlin, Heidelberg, 2007)
20. P. M. Johns, Materials Development For Nuclear Security: Bismuth Triiodide Room Temperature Semiconductor Detectors, (University of Florida, 2017)
21. V.M. Zaletin, Development of semiconductor detectors based on wide-gap materials. At. Energy **97**, 773 (2004)
22. S. Abbaspour, B. Mahmoudian, J. Islamian, Cadmium telluride semiconductor detector for improved spatial and energy resolution radioisotopic imaging. World J. Nucl. Med. **16**, 101 (2017)
23. P.M. Johns, J.C. Nino, Room temperature semiconductor detectors for nuclear security. J. Appl. Phys. **126**, 040902 (2019)
24. B. Zerroumda, H. Ferhati, F. Djeffal, S. Benaggoune, A novel high-performance junctionless 4H-SiC trench MOSFET with improved switching characteristics. Microelectron. Eng. **277**, 112011 (2023)
25. X. Guo, H. Song, Y. Li, P. Wang, S. Liu, Fabrication of 4H–SiC nanoparticles using femtosecond pulsed laser ablation in deionized water. Opt. Mater. (Amst) **132**, 112817 (2022)
26. G.A. Armantrout, S.P. Swierkowski, J.W. Sherohman, J.H. Yee, What can be expected from high-Z semiconductor detectors? IEEE Trans. Nucl. Sci. **24**, 121 (1977)
27. Z. Kang, Y. Zhang, H. Menkara, B.K. Wagner, C.J. Summers, W. Lawrence, V. Nagarkar, CdTe quantum dots and polymer nanocomposites for X-ray scintillation and imaging. Appl. Phys. Lett. **98**, 181914 (2011)
28. P.J. Sellin, Recent advances in compound semiconductor radiation detectors. Nucl. Instrum. Methods Phys. Res. Sect. A Accel. Spectrom. Detect. Assoc. Equip. **513**, 332 (2003)
29. C. Han, E. Sahle-Demessie, E. Varughese, H. Shi, Polypropylene–MWCNT composite degradation, and release, detection and toxicity of MWCNTs during accelerated environmental aging. Environ. Sci. Nano **6**, 1876 (2019)
30. C.V. More, Z. Alsayed, M.S. Badawi, A.A. Thabet, P.P. Pawar, Polymeric composite materials for radiation shielding: a review. Environ. Chem. Lett. **19**, 2057 (2021)
31. H. Spieler, in *" Silicon Detectors " Basic Concepts I*, Lectures on Detector Techniques Stanford Linear Accelerator Center September 1998— February, 1999 (1998).
32. M. O. Schillgalies, *Silicon Photodiodes For Gamma Ray Detection*, First Sens. 1 (2011).
33. M. Turala, Silicon tracking detectors—historical overview. Nucl. Instrum. Methods Phys. Res. Sect. A Accel. Spectrom. Detect. Assoc. Equip. **541**, 1 (2005)
34. G. Lindström, Radiation damage in silicon detectors. Nucl. Instrum. Methods Phys. Res. Sect. A **512**, 30–43 (2003)
35. J.G. Webster, M.R. Squillante, J.F. Christian, and G. Entine, Solid state radiation detectors. Wiley Encycl. Electr. Electron. Eng. **1** (2016).
36. J. Eberth, H.G. Thomas, P.V. Brentano, R.M. Lieder, H.M. Jäger, H. Kämmerfing, M. Berst, D. Gutknecht, R. Henck, Encapsulated Ge detectors: development and first tests. Nucl. Instrum. Methods Phys. Res. Sect. A Accel. Spectrom. Detect. Assoc. Equip. **369**, 135 (1996)
37. W. Adam et al., Review of the development of diamond radiation sensors. Nucl. Instruments Methods Phys. Res. Sect. A Accel. Spectrom. Detect. Assoc. Equip. **434**, 131 (1999)
38. K. Su, Z. Ren, J. Zhang, L. Liu, J. Zhang, Y. Zhang, Q. He, C. Zhang, X. Ouyang, Y. Hao, High performance hydrogen/oxygen terminated CVD single crystal diamond radiation detector. Appl. Phys. Lett. **116**, 092104 (2020)
39. G.R. Fern, P.R. Hobson, A. Metcalfe, D.R. Smith, Performance of four CVD diamond radiation sensors at high temperature. Nucl. Instrum. Methods Phys. Res. Sect. A Accel. Spectrom. Detect. Assoc. Equip. **958**, 162486 (2020)
40. S. Del Sordo, L. Abbene, E. Caroli, A.M. Mancini, A. Zappettini, P. Ubertini, Progress in the development of CdTe and CdZnTe semiconductor radiation detectors for astrophysical and medical applications. Sensors **9**, 3491 (2009)
41. Y. Jia, Y. Shen, X. Sun, Z. Shi, K. Jiang, T. Wu, H. Liang, X. Cui, W. Lü, D. Li, Improved performance of SiC radiation detector based on metal–insulator–semiconductor structures. Nucl. Instrum. Methods Phys. Res. Sect. A Accel. Spectrom. Detect. Assoc. Equip. **997**, 165166 (2021)
42. Y. Eisen, A. Shor, CdTe and CdZnTe room-temperature X-ray and gamma ray detectors and imaging systems. Mater. Res. Soc. Symp. Proc. **487**, 129 (1998)
43. T. Takahashi, S. Watanabe, Recent progress in CdTe and CdZnTe detectors. IEEE Trans. Nucl. Sci. **48**, 950 (2001)
44. M. Sun, D. Zhao, Z. Yin, F. Yang, W. Jie, T. Wang, Material properties and device performance of CdSe radiation detectors. Nucl. Instrum. Methods Phys. Res. Sect. A Accel. Spectrom. Detect. Assoc. Equip. **959**, 163487 (2020)
45. S. Wei et al., Single crystal CdSe X-ray detectors with ultra-high sensitivity and low detection limit. ACS Appl. Mater. Interfaces **12**, 56126 (2020)
46. C. Szeles, CdZnTe and CdTe materials for X-ray and gamma ray radiation detector applications. Phys. Status Solidi **241**, 783 (2004)
47. U.N. Roy, G.S. Camarda, Y. Cui, R. Gul, A. Hossain, G. Yang, J. Zazvorka, V. Dedic, J. Franc, R.B. James, Role of selenium addition to CdZnTe matrix for room-temperature radiation detector applications. Sci. Rep. **9**, 1620 (2019)
48. X. Gao, H. Sun, D. Yang, P. Wangyang, C. Zhang, X. Zhu, Large-area CdZnTe thick film based array X-ray detector. Vacuum **183**, 109855 (2021)
49. A. Datta, J. Fiala, P. Becla, S. Motakef, Stable room-temperature thallium bromide semiconductor radiation detectors. APL Mater. **5**, 106109 (2017)

50. I.B. Oliveira, F.E. Costa, P.K. Kiyohara, M.M. Hamada, Influence of crystalline surface quality on TlBr radiation detector performance. IEEE Trans. Nucl. Sci. **52**, 2058 (2005)
51. K. Hitomi, T. Shoji, K. Ishii, Advances in TlBr detector development. J. Cryst. Growth **379**, 93 (2013)
52. W.R. Willig, Mercury iodide as a gamma spectrometer. Nucl. Instrum. Methods **96**, 615 (1971)
53. K.-T. Kim, J.-H. Kim, M.-J. Han, S.-S. Lee, Y.-J. Heo, G.-S. Cho, B.-I. Min, H.-L. Cho, K.-B. Kim, S.-K. Park, Characterization of a HgI2 dosimeter for the monitoring system of position detection of radioactive sources in gamma-ray projector. Sci. Adv. Mater. **12**, 1502 (2020)
54. M. Schieber, Fabrication of HgI2 nuclear detectors. Nucl. Instrum. Methods **144**, 469 (1977)
55. K.-B. Kim, J.-S. Kim, K.-T. Kim, S.-H. Choi, G.-S. Cho, W.-I. Jang, S. Kwon, Stabilization of mercuric iodide using titanium and silicon oxides. J. Korean Phys. Soc. **76**, 484 (2020)
56. F. Zhuge, P. Luo, T. Zhai, Lead-free perovskites for X-ray detecting. Sci. Bull. **62**, 1491 (2017)
57. K.S. Shah, P. Bennett, M. Klugerman, L. Moy, L. Cirignano, Y. Dmitriyev, M.R. Squillante, F. Olschner, W.W. Moses, in *Lead Iodide Optical Detectors for Gamma Ray Spectroscopy*, 1996 IEEE Nuclear Science Symposium. Conference Record, Vol. 1 (IEEE, 1996), pp. 21–24
58. T. Hayashi, M. Kinpara, J.F. Wang, K. Miraura, M. Isshiki, Growth of ultra-high purity PbI2 single crystal: (1) preparation of high purity PbI2. Cryst. Res. Technol. **43**, 9 (2008)
59. T. Saito, T. Iwasaki, S. Kurosawa, A. Yoshikawa, T. Den, BiI_3 single crystal for room-temperature gamma ray detectors. Nucl. Instrum. Methods Phys. Res. Sect. A Accel. Spectrom. Detect. Assoc. Equip. **806**, 395 (2016)
60. C.C. Stoumpos et al., Crystal growth of the perovskite semiconductor $CsPbBr_3$: a new material for high-energy radiation detection. Cryst. Growth Des. **13**, 2722 (2013)
61. H. Li, F. Meng, C.D. Malliakas, Z. Liu, D.Y. Chung, B. Wessels, M.G. Kanatzidis, Mercury chalcohalide semiconductor Hg3 Se2 Br2 for hard radiation detection. Cryst. Growth Des. **16**, 6446 (2016)
62. H. Needleman, Lead poisoning. Annu. Rev. Med. **55**, 209 (2004)
63. P.A. Beckmann, A review of polytypism in lead iodide. Cryst. Res. Technol. **45**, 455 (2010)
64. C.R. Kant, P. Arun, Controlling the photoluminescence of ZnO: Si nano-composite films by heat-treatment. Mater. Res. Bull. **45**, 1368 (2010)
65. X. Zhao et al., Nanosecond X-ray detector based on high resistivity ZnO single crystal semiconductor. Appl. Phys. Lett. **108**, 171103 (2016)
66. M. Simon, R.A. Ford, A.R. Franklin, S.P. Grabowski, B. Menser, G. Much, A. Nascetti, M. Overdick, M.J. Powell, D.U. Wiechert, in *PbO as Direct Conversion X-Ray Detector Material*, ed. by M.J. Yaffe M.J. Flynn. Medical Imaging 2004: Physics of Medical Imaging, Vol. 5368 (2004), p. 188.
67. C.R. Kant, P. Arun, Film thickness controlled photoluminescence emission in ZnO: Si nanocomposite. Opt. Mater. **35**, 314 (2012)
68. C.R. Kant, P. Arun, White-light emission from annealed ZnO: Si nanocomposite thin films. J. Lumin. **132**, 1744 (2012)
69. J.M. Lobez, T.M. Swager, Radiation detection: resistivity responses in functional Poly(Olefin Sulfone)/carbon nanotube composites. Angew. Chem. Int. Ed. **49**, 95 (2010)
70. N. Kucuk, M. Cakir, N.A. Isitman, Mass attenuation coefficients, effective atomic numbers and effective electron densities for some polymers. Radiat. Prot. Dosim. **153**, 127 (2013)
71. D. Wang, *Semiconductor nanocrystal-polymer composites: using polymers for nanocrystal processing*. Semicond. Nanocrystal Quantum Dots Synth. Assem. Spectrosc. Appl. **171** (2008)
72. D. Bloor, K. Donnelly, P.J. Hands, P. Laughlin, D. Lussey, A metal-polymer composite with unusual properties. J. Phys. D Appl. Phys. **38**, 2851 (2005)
73. A. Barabash, D. Barabash, V. Pertsev, D. Panfilov, Polymer-composite materials for radiation protection. Adv. Intell. Syst. Comput. **983**, 352–360 (2019)
74. A. Upadhyay, S. Karpagam, Movement of new direction from conjugated polymer to semiconductor composite polymer nanofiber. Rev. Chem. Eng. **35**, 351 (2019)
75. S.K. Sharma, R.P. Tandon, V.K. Sachdev, Pre-localized MWCNT network for a low percolation threshold in MWCNT/ABS nanocomposites: experiment and theory. RSC Adv. **4**, 60733 (2014)
76. A.M.S. Galante, O.L. Galante, L.L. Campos, Study on application of PTFE, FEP and PFA fluoropolymers on radiation dosimetry. Nucl. Instrum. Methods Phys. Res. Sect. A Accel. Spectrom. Detect. Assoc. Equip. **619**, 177 (2010)
77. A. Intaniwet, C.A. Mills, M. Shkunov, P.J. Sellin, J.L. Keddie, Heavy metallic oxide nanoparticles for enhanced sensitivity in semiconducting polymer X-ray detectors. Nanotechnology **23**, 235502 (2012)
78. S. Nambiar, E.K. Osei, J.T.W. Yeow, Polymer nanocomposite-based shielding against diagnostic X-rays. J. Appl. Polym. Sci. **127**, 4939 (2013)
79. A.I. Ayesh, B. Salah, L.A. Al-Sulaiti, Production and characterization of flexible semiconducting polymer-nanoparticle composites for X-ray sensors. Radiat. Phys. Chem. **167**, 108233 (2020)
80. S. Nambiar, J.T.W. Yeow, Polymer-composite materials for radiation protection. ACS Appl. Mater. Interfaces **4**, 5717 (2012)
81. D. Nason, L. Keller, The growth and crystallography of bismuth tri-iodide crystals grown by vapor transport. J. Cryst. Growth **156**, 221 (1995)
82. Y.N. Dmitriyev, P.R. Bennett, L.J. Cirignano, M.B. Klugerman, K.S. Shah, in *Bismuth Iodide Crystals as a Detector Material: Some Optical and Electrical Properties*, ed. by R.B. James, R.C. Schirato. Hard X-Ray, Gamma-Ray, and Neutron Detector Physics, Vol. 3768 (1999), p. 521
83. M. Matsumoto, K. Hitomi, T. Shoji, and Y. Hiratate, in *Bismuth iodide (III) crystals for nuclear radiation detectors*, IEEE Nuclear Science Symposium and Medical Imaging Conference, Vol. 4 (IEEE, 2002), pp. 2344–2347
84. A. Garg, M. Tomar, V. Gupta, Synthesis and characterisation of thin films of bismuth triiodide for semiconductor radiation detectors. Conf. Pap. Sci. **2014**, 1 (2014)
85. W. Qiu, G.J. Dudder, X. Zhao, S.S. Perry, J.C. Nino, Interfacial reactivity of Au, Pd, and Pt on BiI_3 (001): implications for electrode selection. ACS Appl. Mater. Interfaces **3**, 1910 (2011)
86. P.M. Johns, J.E. Baciak, and J.C. Nino, *Enhanced gamma ray sensitivity in bismuth triiodide sensors through volumetric defect control.* Appl. Phys. Lett. **109** (2016)
87. P.M. Johns, S. Sulekar, S. Yeo, J.E. Baciak, M. Bliss, J.C. Nino, Superheating suppresses structural disorder in layered BiI_3 semiconductors grown by the Bridgman method. J. Cryst. Growth **433**, 153 (2016)
88. T.R. Devidas, N.V. Chandra Shekar, C.S. Sundar, P. Chithaiah, Y.A. Sorb, V.S. Bhadram, N. Chandrabhas, K. Pal, U.V. Waghmare, C.N.R. Rao, Pressure-induced structural changes and insulator-metal transition in layered bismuth triiodide, BiI_3: a combined experimental and theoretical study. J. Phys. Condens. Matter **26**, 275502 (2014)
89. J. Trotter, T. Zobel, The crystal structure of SbI_3 and BiI_3. Zeitschrift Für Krist. Cryst. Mater. **123**, 81 (1966)
90. B.J. Curtis, H.R. Brunner, The crystal growth of bismuth iodide. Mater. Res. Bull. **9**, 715 (1974)
91. C.C. Coleman, H. Goldwhite, W. Tikkanen, a review of intercalation in heavy metal iodides. Chem. Mater. **10**, 2794 (1998)

92. M. Schlüter, M.L. Cohen, S.E. Kohn, C.Y. Fong, Electronic structure of BiI_3. Phys. Status Solidi **78**, 737 (1976)
93. Y. Kaifu, T. Komatsu, T. Aikami, Optical properties of BiI_3 single crystals. Nuovo Cim. B Ser. **11**(38), 449 (1977)
94. Y. Kaifu, Excitons in layered BiI_3 single crystals. J. Lumin. **42**, 61 (1988)
95. T. Karasawa, T. Komatsu, Y. Kaifu, Zone-folding effects on phonons and excitons in polytypic BiI_3 single crystals. Solid State Commun. **44**, 323 (1982)
96. D.G.S.A.A. Kikineshi, Localized states and electron-hole processes in BiI_3 crystals. Phys. Stat. Sol. **12**, 299 (1972)
97. J. Seco, B. Clasie, M. Partridge, Review on the characteristics of radiation detectors for dosimetry and imaging. Phys. Med. Biol. **59**, R303 (2014)
98. I.F. Kopinets, S.V. Mikulaninets, I.D. Turyanitsa, D.V. Chepur, Effect of oxygen adsorption on the properties of bismuth triiodide single crystals. Sov. Phys. J. **12**, 1118 (1972)
99. B. Wagner, A. Huttner, D. Bischof, A. Engel, G. Witte, J. Heine, Chemical surface reactivity and morphological changes of bismuth triiodide (BiI_3) under different environmental conditions. Langmuir **36**, 6458 (2020)
100. N.C. Greenham, X. Peng, A.P. Alivisatos, Charge separation and transport in conjugated polymer/cadmium selenide nanocrystal composites studied by photoluminescence quenching and photoconductivity. Synth. Met. **84**, 545 (1997)
101. T.J. Hajagos, C. Liu, N.J. Cherepy, Q. Pei, High-Z sensitized plastic scintillators: a review. Adv. Mater. **30**, 1706956 (2018)
102. G. Aydın, Simulation study for the energy resolution performances of homogenous calorimeters with scintillator-photodetector combinations. Adv. High Energy Phys. **2018**, 1 (2018)
103. M.F. L'annunziata, in *Nuclear Radiation, Its Interaction With Matter And Radioisotope Decay*, Handbook of Radioactivity Analysis (Elsevier, 2003), pp. 1–121
104. M.J. Berger, J.H. Hubbell, S.M. Seltzer, J. Chang, J.S. Coursey, R. Sukumar, D.S. Zucker, K. Olsen, XCOM: Photon Cross Section Database (version 1.5). (National Institute of Standards and Technology, Gaithersburg, 2010), http://physics.nist.gov/xcom. Accessed 27 Oct 2023
105. N.J. Podraza, W. Qiu, B.B. Hinojosa, M.A. Motyka, S.R. Phillpot, J.E. Baciak, S. Trolier-McKinstry, J.C. Nino, Band gap and structure of single crystal BiI_3: resolving discrepancies in literature. J. Appl. Phys. **114**, 033110 (2013)
106. R. Minder, G. Ottaviani, C. Canali, Charge transport in layer semiconductors. J. Phys. Chem. Solids **37**, 417 (1976)
107. Lovkush, C. Ravi Kant, P. Arun, Tunability of surface plasmon resonance peaks in CsI: Ag films by growth conditions. Plasmonics **15**, 735 (2020)
108. L. Fornaro, I. Aguiar, A. Noguera, M. Perez, M. Rodriguez, Improvements on bismuth tri-iodide platelets for room temperature X-ray detection, In 2006 IEEE Nuclear Science Symposium Conference Record (IEEE, 2006), pp. 3616–3621
109. A. T. Lintereur, W. Qiu, J. C. Nino, and J. E. Baciak, in *Iodine Based Compound Semiconductors for Room Temperature Gamma-Ray Spectroscopy*, ed. by C.S. Halvorson, D. Lehrfeld, T.T. Saito.*Optics and Photonics in Global Homeland Security IV*, Vol. 6945 (2008), p. 694503
110. K. Oh, M.-S. Yun, S. Cho, M. Kim, Y. Kim, Y. Kim, J.-U. Sin, S. Nam, Laminate structure detectors for low dark current with photoconductors in digital X-ray imaging. Nucl. Instrum. Methods Phys. Res. Sect. A Accel. Spectrom. Detect. Assoc. Equip. **607**, 158 (2009)
111. M. Ikeda, T. Oka, K. Mori, and M. Atsuta, *Study of dark current blocking layer for BiI/Sub3/X-Ray detector film*, In *IEEE Symposium Conference Record Nuclear Science 2004.*, Vol. 7 (IEEE, 2004), pp. 4520–4523.
112. L. Fornaro, A. Cuna, A. Noguera, M. Perez, L. Mussio, Growth of bismuth tri-iodide platelets for room temperature X-ray detection. IEEE Trans. Nucl. Sci. **51**, 2461 (2004)
113. I. Aguiar, S. Kröger, L. Fornaro, Bismuth tri-iodide polycrystalline films for X-ray direct and digital imagers. Nucl. Instruments Methods Phys. Res. Sect. A Accel. Spectrometers, Detect. Assoc. Equip. **610**, 332 (2009).
114. L. F. Ivana Aguiar, Alvaro Olivera, Heinkel Bentos Pereira, in *Development of a novel Ionizing radiation detector based in hydrothermally synthesized BiI_3 Nanostructures*, XIV Brazil MRS Meeting (2015), pp. 1–2
115. N.S. Edwards and D. S. McGregor, in *Charge collection efficiency mapping of a frisch-collared BiI_3 device*, In *2014 IEEE Nuclear Science Symposium and Medical Imaging Conference (NSS/MIC)* (IEEE, 2014), pp. 1–4
116. S.S. Gokhale, H. Han, J.E. Baciak, J.C. Nino, K.A. Jordan, Growth, fabrication, and testing of bismuth tri-iodide semiconductor radiation detectors. Radiat. Meas. **74**, 47 (2015)
117. H. Han, M. Hong, S.S. Gokhale, S.B. Sinnott, K. Jordan, J.E. Baciak, J.C. Nino, Defect engineering of BiI_3 single crystals: enhanced electrical and radiation performance for room temperature gamma-ray detection. J. Phys. Chem. C **118**, 3244 (2014)
118. A.T. Lintereur, W. Qiu, J.C. Nino, J. Baciak, Characterization of bismuth tri-iodide single crystals for wide band-gap semiconductor radiation detectors. Nucl. Instrum. Methods Phys. Res. Sect. A Accel. Spectrom. Detect. Assoc. Equip **652**, 166 (2011)
119. S.S. Gokhale, H.S. Han, O. Pelaez, J.E. Baciak, J.C. Nino, K.A. Jordan, Fabrication and testing of antimony doped bismuth triiodide semiconductor gamma-ray detectors. Radiat. Meas. **91**, 1 (2016)
120. H. Sun, X. Zhu, P. Wangyang, X. Gao, S. Zhu, B. Zhao, Preparation and characterization of free-standing—BiI_3 single-crystal flakes for X-ray detection application. J. Mater. Sci. Mater. Electron. **29**, 20003 (2018)
121. P. Praveenkumar, G.D. Venkatasubbu, P. Thangadurai, T. Prakash, Nanocrystalline bismuth oxyiodides thick films for X-ray detector. Mater. Sci. Semicond. Process. **104**, 104686 (2019)
122. Y. Liu, H. Sun, D. Yang, P. Wangyang, X. Gao, Z. Gou, X. Zhu, Electrical properties of X-ray detector based on bismuth Triiodide single crystal with electrode configuration considering. Mater. Res. Express **6**, 055902 (2019)
123. R. Chaudhari, A. Garg, K. Singh, M. Tomar, V. Gupta, C. RaviKant, Bismuth tri-iodide-polystyrene composite for x-rays switching applications at room temperature. Radiat. Phys. Chem. **186**, 109538 (2021)
124. C. De Blasi, S. Galassini, C. Manfredotti, G. Micocci, L. Ruggiero, A. Tepore, Trapping levels in PbI2. Solid State Commun. **25**, 149 (1978)
125. A. Kargar, H. Kim, L. Cirignano, K. Shah, in *The effect of guard ring on leakage current and spectroscopic performance of TlBr planar detector*, ed. by G. P. Grim and H. B. Barber. Radiation Detectors: Systems and Applications XV, Vol. 9215 (2014), p. 92150E
126. H.Y. Cho, J.H. Lee, Y.K. Kwon, J.Y. Moon, C.S. Lee, Measurement of the drift mobilities and the mobility-lifetime products of charge carriers in a CdZnTe crystal by using a transient pulse technique. J. Instrum. **6**, C01025 (2011)
127. G. Ariño-Estrada, M. Chmeissani, G. de Lorenzo, M. Kolstein, C. Puigdengoles, J. García, E. Cabruja, Measurement of mobility and lifetime of electrons and holes in a Schottky CdTe diode. J. Instrum. **9**, C12032 (2014)
128. P.J. Sellin, Thick film compound semiconductors for X-ray imaging applications. Nucl. Instrum. Methods Phys. Res. Sect. A Accel. Spectrom. Detect. Assoc. Equip. **563**, 1 (2006)

129. W. Koehler, M. Streicher, S. O'Neal, Z. He, A correction factor to the two-bias method for determining mobility-lifetime products in pixelated detectors. IEEE Trans. Nucl. Sci. **63**, 1832 (2016)
130. H.M. Thirimanne et al., High sensitivity organic inorganic hybrid X-ray detectors with direct transduction and broadband response. Nat. Commun. **9**, 2926 (2018)
131. R.R. Karthieka, R.N. Begum, T. Prakash, Direct conversion X-ray sensing nature of Bismuth (III) Iodide thick films. Chin. J. Phys. **71**, 643 (2021)
132. L. Mao, Y. Li, L. Yu, X. Li, J. Zhang, Stable and printable direct X-ray detectors based on micropyramid ω-Bi_2O_3 with low detection limit. IEEE Trans. Electron Devices **68**, 3411 (2021)
133. M. Thompson, S.L.R. Ellison, R. Wood, Harmonized guidelines for single-laboratory validation of methods of analysis (IUPAC Technical Report). Pure Appl. Chem. **74**, 835 (2002)
134. N.J. Cherepy et al., in *Performance of Europium-doped strontium iodide, transparent ceramics and bismuth-loaded polymer scintillators*, ed. by L.A. Franks, R.B. James, and A. Burger. Hard X-Ray, Gamma-Ray, and Neutron Detector Physics XIII, Vol. 8142 (2011), p. 81420W
135. A. Salleo, R.J. Kline, D.M. DeLongchamp, M.L. Chabinyc, Microstructural characterization and charge transport in thin films of conjugated polymers. Adv. Mater. **22**, 3812 (2010)
136. R. Chaudhari, C. RaviKant, A review on BiI_3 perovskites and composites for direct X-ray detection. Sens. Actuators A Phys. **346**, 113863 (2022)
137. R. Chaudhari, C.R. Kant, A. Garg, Polymer-BiI_3 composites for high-performance, room temperature, direct X-ray detectors. MRS Commun. **12**, 358–364 (2022)
138. R. Chaudhari, C.R. Kant, Defects studies of BiI_3-polymer composites with carbon fillers to achieve better charge transportation for direct X-ray detectors. Mater. Sci. Semicond. Process. **163**, 107555 (2023)
139. R. Chaudhari, S. Kumar Sharma, C. Ravi Kant, A. Garg, Investigations on low energy X-ray induced strong radiation-matter interaction phenomena in polymer-BiI_3 hybrid materials for room temperature radiation detectors. Mater. Today Proc. **67**, 478 (2022)
140. X. Zheng, W. Zhao, P. Wang, H. Tan, M.I. Saidaminov, S. Tie, L. Chen, Y. Peng, J. Long, W.H. Zhang, Ultrasensitive and stable X-ray detection using zero-dimensional lead-free perovskites. J. Energy Chem. **49**, 299 (2020)